*Journal of Engineering Mathematics* **27**: 245–264, 1993.



# Swirling free surface flow in cylindrical containers

A. SIGINER and R. KNIGHT
*Department of Mechanical Engineering, Auburn University, Auburn, AL 36849, USA*

Received 25 February 1992; accepted in revised form 7 November 1992

**Abstract.** Free surface flow in a cylindrical container with steadily rotating bottom cap is investigated. A regular domain perturbation in terms of the angular velocity of the bottom is used. The flow field is made up of the superposition of azimuthal and meridional fields. The meridional field is solved both by biorthogonal series and a numerical algorithm. The free surface on the liquid is determined at the lowest significant order. The aspect ratio of the cylinder may generate a multiple cell structure in the meridional plane which in turn shapes the free surface.

## I. Introduction

Rotating flow systems are encountered frequently in nature and in technological applications. Large bodies of fluid form rotating systems in the atmosphere and the oceans. Tornadoes and the swirling flows around the Great Red Spot on the planet Jupiter are striking examples of such systems. In technology, applications may be found in areas as diverse as lubrication and turbo-machinery. New applications are emerging in the manufacture of crystals with potential use in computer memories and in rotating cavity flows in computer disc drives.

The investigations in this broad field were initiated by Von Kármán [1] who considered the flow in the half plane above a steadily rotating infinite disc and reduced the Navier–Stokes equations to a pair of coupled ordinary differential equations by a similarity transformation, thus obtaining an exact representation of the Navier–Stokes equations in a more tractable form which he left unsolved. The first attempts to numerically solve these equations were made by Cochran [2] and Bödewadt [3]. The last author considered the flow above an infinite disk at rest driven by the fluid at infinity in solid body rotation. Two seminal contributions were made in the early fifties by Batchelor [4] and Stewartson [5], in particular to the case of the flow between parallel, infinite, coaxial disks. Navier–Stokes equations are again reducible in this case to a set of coupled ordinary differential equations by Von Kármán transformation.

Batchelor argued that if the discs rotate in the same sense, possibly with different angular velocities, the main body of the fluid between the discs would be in solid body rotation at an angular velocity in between those of the discs whereas if they rotate in opposite directions the main body would again be in solid body rotation with a two cell structure separated by a shear layer with boundary layers on the rotating discs. The faster disc acts as a centrifugal fan, and the discs are attracted to each other indicating that the pressure is reduced in the main body of fluid. In the later paper, Stewartson [5] claimed that although experimentally and theoretically Batchelor's predictions for the discs rotating in the same sense are verified, for the discs rotating in opposite directions the main body of the fluid is almost motionless except for a slight inward radial velocity with the discs repelling each other.

These predictions are also relevant to the related class of flows taking place between finite

discs enclosed by a cylinder as shown by Brady and Durlofsky [6], and also in free surface flows in a cylinder driven from the bottom as indicated by our computations. In the ensuing decades a flurry of papers were published dealing with flow between infinite discs. A good review of the state of the research in this area is published by Zandbergen and Dijkstra [7]. The interest in the field is not anywhere close to subside not only because Navier-Stokes equations are represented exactly by a coupled pair of ordinary differential equations, which is a feat in itself, but the solution of those equations appears to be nonunique.

A related class of problems is formed by flows between rotating discs enclosed by a cylinder. The presence of side walls precludes the use of the similarity approach. The full Navier-Stokes equations must be solved and the non-uniqueness, which seems to be a prominent feature of the flow between infinite discs, is removed. Schultz-Grunow [8] studied a flow problem in this class generated by a rotating disc and a stationary sheath followed by other papers, relatively few in numbers when compared to the activity concerning flow between infinite discs. In particular, the work of Pao [9] who developed asymptotic solutions in terms of Bessel functions for this type of rotating flows should be mentioned.

The slightly different problem of the unsteady fluid motion with a free surface in a rotating cylindrical tank subjected to a step change in the rotation rate is of interest, in particular, to geophysical fluid dynamicists because it provides a simplified model of the large scale atmospheric and oceanic circulation. The effect of the spin-up or spin-down of a homogeneous fluid in a rotating cylinder has been recently investigated by Cederlöf [10]; O'Donnell and Linden [11].

The related problem of the free surface flow in cylindrical cavities driven from the bottom is investigated in this paper. The only work known to us in the literature dealing with free surface flows in a similar geometry with the same driving conditions is by Hyun [12]. He neglects the effect of a deformable free surface in determining the flow field which, contrary to his arguments, may be considerable. His numerical solution which uses the vorticity-stream function formulation is valid for a rectangular domain in the meridional plane with shear free rigid flat top. The free surface shape is not determined, and aspect ratios larger than one are not considered. We solve the flow field with a deformable, shear free top boundary for aspect ratios larger and smaller than unity, determine the shape of the free surface taking into account surface tension, trace the evolution of the flow field and the free surface shape with changing aspect ratio, and bring out the effect of the velocity singularity at the junction of the bottom disk and side wall.

A regular perturbation in terms of the angular velocity of the bottom cover is used to perturb simultaneously both the inertial non-linearity and the unknown flow domain. Flow variables are expanded in power series in $\Omega$, the angular velocity of the cover. The successive linear problems defining the coefficients of the power series up to and including the second order are solved in the cylindrical domain with flat top and the solution is continued to the physical domain with deformed top. The flow field is broken, at the lowest significant orders, into the superposition of an azimuthal field, a vertically stratified viscometric flow, and a meridional field created by the bottom cover acting as a centrifugal fan. The primary field, the azimuthal flow, is a first order effect in $\Omega$, the angular velocity of the bottom. The secondary field, the meridional flow, is a second order effect in $\Omega$. The hydrostatic nature of the pressure field is not altered at the first order and the first correction is obtained at the second order. A balance equation between the stress jump in the normal direction to the free surface and surface tension forces yields the shape of the free surface. The first correction to the flatness of the top is obtained at the second order. The correction is

dependent on the deviation of the pressure field from hydrostatic distribution and any unbalanced shear stresses at the top, both of which are absent and present at the first and second orders respectively.

The meridional flow is determined by a fourth order inhomogeneous ODE defined by the square of the Beltrami-Stokes operator. An attempt is made to solve the equation by complex biorthogonal series. But although convergence in the interior is quite rapid and close to the solution, convergence to the boundary data cannot be obtained in a neighborhood of the corner where the disk joins the side wall, although the data is reasonably well represented over the rest of the boundary. The solution is brought about instead by way of a numerical algorithm the details of which are presented.

Cylinder aspect ratio is important in shaping the meridional field and the free surface. A multiple cell structure may take place and the surface may rise near the axis and sink near the wall contrary to intuitive deduction.

Azimuthal velocity level lines together with vorticity and streamline contours in the meridional plane are presented for aspect ratios ranging from tall to almost flat cylinders. Free surface profiles on the liquid at different aspect ratios and high and low values of the interfacial surface tension are also presented.

Batchelor and Stewartson type of motions are quite relevant to the problem investigated in this paper. For tall cylinders, liquid away from the wall is almost motionless with a slight inward radial velocity in the meridional plane close to the top thereby invoking a Stewartson type of field whereas for cylinders with low aspect ratio the meridional flow is basically confined to a small region close to the end wall, and away from the end wall the primary azimuthal flow displays a horizontally stratified shear field towards the end wall akin to solid body motion and quite reminiscent of the Batchelor type of field.

## II. Mathematical formulation

The physical domain $D_\Omega$ is shown in Fig. 1.

$$D_\Omega = \{R, \theta, Z | 0 \leq R \leq a, 0 < \theta \leq 2\pi, -d \leq Z \leq h(r)\} .$$

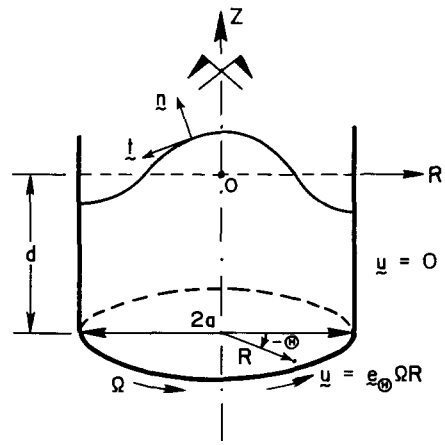


*Fig. 1.* Flow configuration.

The motion takes place in a cylindrical container of radius $a$ with fixed sidewall the bottom cover of which rotates at constant angular velocity $\Omega$. Liquid in the container at rest stands to a depth $d$. The coordinate frame is located on the surface of the liquid at rest with the origin on the axis of symmetry. The field equations read

$$\rho \frac{D\mathbf{u}}{Dt} = -\nabla\Phi + \mu\nabla^2\mathbf{u}\,, \qquad \nabla\cdot\mathbf{u} = 0\,, \qquad \Phi = p + \rho g Z \quad \in D_\Omega \tag{1}$$

with a modified pressure field $\Phi$ and subject to no-slip conditions on the solid walls

$$\mathbf{u}(a, Z) = 0\,, \qquad \mathbf{u}(R, -d) = \mathbf{e}_\theta \Omega R\,, \qquad \mathbf{u}(0, Z) < +\infty\,. \tag{2}$$

The surface $h(R;\Omega)$ on the liquid is traction free and there is no velocity component perpendicular to it.

$$S_{n\theta} = S_{Z\theta} - h_{,R} S_{R\theta} = 0\,, \tag{3}$$

$$S_{nt} = h_{,R}(S_{ZZ} - S_{RR}) + (1 - h_{,R}^2) S_{RZ} = 0\,, \tag{4}$$

$$w|_{Z=h} = h_{,R} u\,, \qquad u = \mathbf{e}_R \cdot \mathbf{u}\,, \qquad w = \mathbf{e}_Z \cdot \mathbf{u}\,. \tag{5}$$

**S**, $n$ and $t$ represent the extra-stress tensor and the normal and tangential directions to the deformed free surface respectively. Mass conservation takes the form

$$\int_0^a Rh(R;\Omega)\,\mathrm{d}R = 0\,, \tag{6}$$

which fixes the constant the pressure field is specified up to.

The inertial nonlinearity in $(1)_1$ and the unknown flow domain $D_\Omega$ are perturbed simultaneously. A regular domain perturbation in terms of the angular velocity $\Omega$ of the bottom cap is used. Flow variables are formally expanded into power series whose coefficients are computed as solutions of linear problems in the rest state $D_0$.

$$D_0 = \{r, \theta, z \,|\, 0 \leqslant r \leqslant a, 0 \leqslant \theta < 2\pi, -d \leqslant z \leqslant 0\}\,.$$

Rest state coordinates $(r, \theta, z)$ are different from coordinates $(R, \theta, Z)$ in the physical domain $D_\Omega$. Symmetries of the problem as defined require that the velocity components in the meridional plane $(u, w)$, the reduced pressure field $\Phi$ and the interface $h$ are even functions of $\Omega$ whereas the azimuthal velocity component $v$ is an odd function of it. The solution may be assumed to be represented in $D_\Omega$ either by

$$\mathbf{u}(R, \theta, Z; \Omega) = \sum_1^\infty \frac{\Omega^n}{n!} \frac{\mathrm{d}^n}{\mathrm{d}\Omega^n} \mathbf{u}(r, \theta, z)|_{\Omega=0}\,, \tag{7a}$$

$$\Phi(R, \theta, Z; \Omega) = \sum_1^\infty \frac{\Omega^{2n}}{2n!} \frac{\mathrm{d}^{2n}}{\mathrm{d}\Omega^{2n}} \Phi(r, \theta, z)|_{\Omega=0}\,, \tag{7b}$$

$$h(R;\Omega) = \sum_1^\infty \frac{\Omega^{2n}}{2n!} \frac{\mathrm{d}^{2n}}{\mathrm{d}\Omega^{2n}} h(r)|_{\Omega=0}\,, \tag{7c}$$

or by

$$\mathbf{u}(R, \theta, Z; \Omega) = \sum_1^\infty \frac{\Omega^n}{n!} \frac{\partial^n}{\partial \Omega^n} \mathbf{u}(r, \theta, z)|_{\Omega=0}\,, \tag{8a}$$

$$\Phi(R, \theta, Z; \Omega) = \sum_1^\infty \frac{\Omega^{2n}}{2n!} \frac{\partial^{2n}}{\partial \Omega^{2n}} \Phi(r, \theta, z)|_{\Omega=0}\,, \tag{8b}$$

$$h(R; \Omega) = \sum_1^\infty \frac{\Omega^{2n}}{2n!} \frac{\partial^{2n}}{\partial \Omega^{2n}} h(r)|_{\Omega=0}\,. \tag{8c}$$

If (7a,b,c) are used the coefficients of the series are computed in $D_0$, the mapping which connects $D_\Omega \leftrightarrow D_0$ is inverted, and the rest state variables in (7a,b,c) are replaced by the variables in $D_\Omega$ to represent the solution in $D_\Omega$. On the other hand if (8a,b,c) are used, the coefficients in the series which are determined in $D_0$ are continued analytically to $D_\Omega$ much like in Stokes' water wave theory and $(r, \theta, z)$ replaced by $(R, \theta, Z)$. Joseph & Sturges [13] show that the series (7a,b,c) after the inversion of the mapping and the series (8a,b,c) after $(r, \theta, z) \rightarrow (R, \theta, Z)$ represent the same functions and the infinite sums are identical. But partial sums with the same number of terms are different, and the question of which series is the optimum representation is open.

The field equations (1) are identities in the parameter $\Omega$ and the coordinates $(R, \theta, Z) \in D_\Omega$. It is easy to show that if $(1)_{1,2}$ are designated by $\mathscr{F}_{1,2}$ one has

$$\frac{\mathrm{d}^n}{\mathrm{d}\Omega^n} \mathscr{F}_i = \frac{\partial^n}{\partial \Omega^n} \mathscr{F}_i\,; \quad i = 1, 2\,. \tag{9}$$

But the interface conditions (3, 4, 5) are not identities in $Z \in D_\Omega$, (9) does not apply and substantial derivatives must be used. In the same vein as $h(R; \Omega)$ is not a function of $Z$ the series (7c) and (8c) are identical even for a finite number of terms.

The shape of the free surface on the liquid is obtained by an application of the classical theory of surface tension. The jump in normal stress across the surface is balanced by surface tension forces.

$$\sigma J = \mathbf{n} \cdot [\mathbf{T}]\mathbf{n}\,, \qquad \mathbf{T} = -p\mathbf{I} + \mathbf{S}\,, \tag{10}$$

where $p$, $\sigma$, $J$, $\mathbf{T}$, $\mathbf{S}$ and $\mathbf{n}$ represent the mechanical pressure, the surface tension, the mean curvature at the interface, the total stress, the deviatoric stress and the unit normal vector to the deformed free surface respectively. The brackets indicate the jump in the total stress across the surface. Equation $(10)_1$ yields

$$\frac{\sigma}{R}\left(\frac{Rh_{,R}}{1 + h_{,R}^2}\right)_{,R} = S_{nn} - p + p_a \tag{11}$$

where $p_a$ represents the atmospheric pressure on the surface.

### *II. 1. First order solution*

Using (1,2), (7a,b) and (9) we obtain

$$\Delta \mathbf{u}^{(1)} = 0\,, \qquad \nabla \cdot \mathbf{u}^{(1)} = 0 \quad \in D_0\,, \tag{12}$$

$$\mathbf{u}^{(1)}(a, z) = 0\,, \qquad \mathbf{u}^{(1)}(r, -d) = \mathbf{e}_\theta r\,, \qquad \mathbf{u}^{(1)}(0, z) < +\infty\,, \tag{13}$$

where the notation $(\cdot)^{(n)}$ indicates the $n$th order partial derivative with respect to $\Omega$ evaluated at $\Omega = 0$. The conditions (3, 4, 5) on the free surface $Z = h(R; \Omega)$ give

$$S^{(1)}_{z\theta}|_{z=0} = S^{(1)}_{rz}|_{z=0} = w^{(1)}|_{z=0} = 0\,, \tag{14}$$

due to

$$\frac{\mathrm{d}^n h}{\mathrm{d}\Omega^n} = \frac{\partial^n h}{\partial \Omega^n}\,, \qquad h^{(0)} = 0\,.$$

Realizing that

$$\mathbf{u}^{(1)}(r, \theta, z; \Omega) = -\mathbf{u}^{(1)}(r, \theta, z; -\Omega)\,, \qquad \mathbf{u}^{(1)} = \mathbf{e}_\theta v^{(1)}(r, z)\,,$$

we introduce dimensionless rest state coordinates

$$\xi = \frac{r}{a}\,, \qquad \eta = \frac{z}{a}\,, \qquad \delta = \frac{d}{a}\,,$$

and reformulate the problem (12, 13, 14) in terms of a dimensionless velocity $V = v^{(1)}/a$

$$\frac{1}{\xi}(\xi V_{,\xi})_{,\xi} - \frac{V}{\xi^2} + V_{,\eta\eta} = 0\,, \qquad V(0, \eta) = V(1, \eta) = 0\,, \qquad V(\xi, -\delta) = \xi\,.$$

Separating variables

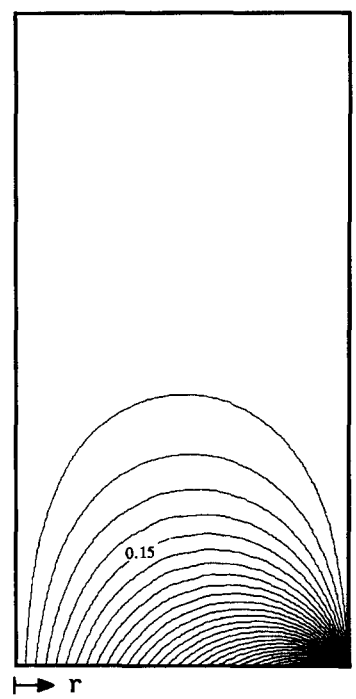


*Fig. 2.* Lines of constant azimuthal velocity; aspect ratio is two.

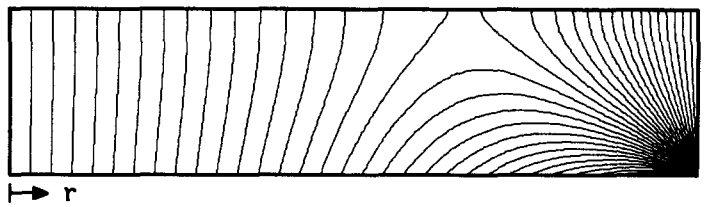


*Fig. 3.* Lines of constant azimuthal velocity; aspect ratio is one fourth.

$$V(\xi,\eta)=\chi(\xi)\zeta(\eta)\,,$$

$$\chi_{,\xi\xi}+\frac{1}{\xi}\chi_{,\xi}-\left(\frac{1}{\xi^2}-A_k^2\right)\chi=0\,,\qquad \chi(1)=0\,,\qquad \chi(0)\text{ bounded}\,, \tag{15}$$

$$\zeta_{,\eta\eta}-A^2\zeta=0\,,\qquad \zeta_{,\eta}(0)=0\,,\qquad \zeta(-\delta)=1\,. \tag{16}$$

The solutions of (15) and (16) combine to yield

$$V(\xi,\eta)=\sum_1^\infty C_k J_1(A_k\xi)Ch(A_k\eta) \tag{17}$$

$$C_k=\frac{2}{A_k J_2(A_k)Ch(-A_k\delta)}\,,\qquad J_1(A_k)=0\,, \tag{17a}$$

with the first and second order Bessel functions $J_1$ and $J_2$. Convergence of the series (17) to the ramp function on the bottom cover is very good and although the series converge to zero at the corner $(1,-\delta)$, the neighborhood $(1-\varepsilon,-\delta)$ of the corner where the series differ from the data may be made very small even with relatively few terms if Cesaro sums $\bar{V}_N$ are used in the summation (17).

$$\bar{V}_N(\xi,-\delta)=\frac{1}{N+1}\sum_1^N V_M(\xi,-\delta)\,,\qquad V_M(\xi,-\delta)=\sum_1^M\frac{2J_1(A_m\xi)}{A_m J_2(A_m)}\,.$$

The first order solution represents a vertically stratified azimuthal field with no alteration to the hydrostatic pressure field. Equation (11) which gives the shape of the surface has no driving terms, and the surface remains flat at this order. Level lines of this primary, vertically stratified shear field are given in Figs. 2–3 for some representative cylinder aspect ratios. These representations are valid both in $D_0$ and $D_\Omega$ because the interface remains flat at this order.

### *II. 2. Second order solution*

The Stokes problem at this order is derived through (1, 2, 3, 4, 5), (7a,b,c) and (9)

$$2\rho\mathbf{u}^{(1)}\cdot\nabla\mathbf{u}^{(1)}=-\nabla\Phi^{(2)}+\mu\,\Delta\mathbf{u}^{(2)}\,,\qquad \nabla\cdot\mathbf{u}^{(2)}=0\text{ in }D_0\,, \tag{18}$$

$$\mathbf{u}^{(2)}(a,z)=0\,,\qquad \mathbf{u}^{(2)}(r,-d)=0\,,\qquad \mathbf{u}^{(2)}(0,z)<+\infty\,, \tag{19}$$

$$S^{(2)}_{z\theta}|_{z=0}=S^{(2)}_{rz}|_{z=0}=w^{(2)}|_{z=0}=0\,. \tag{20}$$

Symmetry considerations require

$$\mathbf{u}^{(2)}(r, \theta, z; \Omega) = \mathbf{u}^{(2)}(r, \theta, z; -\Omega) ,$$

$$\mathbf{u}^{(2)} = \mathbf{e}_r u^{(2)}(r, z) + \mathbf{e}_z v^{(2)}(r, z) .$$

We introduce a stream function $\psi^{(2)}(r, z)$ and satisfy $(18)_2$ identically. Defining a dimensionless $\Psi(\xi, \eta)$ in terms of the dimensionless rest state variables $(\xi, \eta)$

$$\Psi(\xi, \eta) = \frac{\psi^{(2)}(r, z)\mu}{\rho a^5} ,$$

we transform $(18)_1$ into

$$L^2\Psi = 2(V^2)_{,\eta} , \qquad L = \xi\left(\frac{1}{\xi}(\cdot)_{,\xi}\right)_{,\xi} + (\cdot)_{,\eta\eta} , \tag{21a}$$

subject to

$$\Psi(1, \eta) = \Psi_{,\xi}(1, \eta) = \Psi(\xi, -\delta) = \Psi_{,\eta}(\xi, -\delta) = 0 , \tag{21b}$$

$$\Psi_{,\eta\eta}(\xi, 0) = \Psi(\xi, 0) = \Psi(0, \eta) = \Psi_{,\xi}(0, \eta) = 0 , \tag{21c}$$

obtained from (19) and (20), respectively. The meridional flow problem defined by (21a,b,c) may be solved by biorthogonal series if a particular integral can be found and $(21a)_1$ is reduced to a homogeneous equation. Considerable search yields a particular solution to $(21a)_1$

$$\Psi_p = \sum_m \sum_n \left(f_{mn}(\xi)\mathrm{Sh}(A_m + A_n)\eta - f^*_{mn}(\xi)\mathrm{Sh}(A_m - A_n)\eta\right) , \tag{22}$$

$$f_{mn}(\xi) = 2\xi^2 D_{mn}(J_{1m}J_{1n} - J_{om}J_{on}) + E_{mn}\xi(A_m J_{on}J_{1m} - A_n J_{1n}J_{om}) ,$$

$$f^*_{mn}(\xi) = 2\xi^2 D^*_{mn}(J_{1m}J_{1n} + J_{om}J_{on}) - E^*_{mn}\xi(A_m J_{on}J_{1m} - A_n J_{1n}J_{om}) ,$$

$$D_{mn} = \frac{C_m C_n A_n}{2(A_m + A_n)^2} , \qquad E_{mn} = \frac{A_n - A_m}{A_n A_m (A_n + A_m)} ,$$

$$J_{lk} = J_l(A_k\xi), l = 0, 1, k = 0, \ldots, \infty ,$$

$$D^*_{mn} = \frac{C_m C_n A_n}{2(A_m - A_n)^2} , \qquad E^*_{mn} = \frac{A_n + A_m}{A_n A_m (A_n - A_m)} .$$

The double summation in (22) is taken over first order eigenvalues $A_k$ which are defined in (17a) together with $C_n$. Then $(21a)_1$ and (21b,c) may be put in the following form

$$\Psi = \Psi^* + \Psi_p , \qquad \Psi^* = \Psi_1 + \Psi_2 ,$$

$$L^2\Psi_1 = 0 \quad \in D_0 , \tag{23}$$

$$\Psi_1(\xi, 0) = \Psi_{1,\eta\eta}(\xi, 0) = \Psi_1(1, \eta) = \Psi_{1,\xi}(1, \eta) = \Psi_{1,\xi}(0, \eta) = \Psi_1(0, \eta) = 0 , \tag{24}$$

$$\Psi_1(\xi, -\delta) = -\sum_m \sum_n \left(f_{mn}(\xi)\mathrm{Sh}(A_m + A_n)\delta + f^*_{mn}(\xi)\mathrm{Sh}(A_m - A_n)\delta\right) , \tag{25}$$

$$\Psi_{1,\eta}(\xi, -\delta) = \sum_m \sum_n ((A_m + A_n) f_{mn}(\xi) \mathrm{Ch}(A_m + A_n)\delta + (A_m - A_n) f^*_{mn}(\xi) \mathrm{Ch}(A_m - A_n)\delta), \tag{26}$$

$$L^2 \Psi_2 = 0 \quad \in D_0, \tag{27}$$

$$\Psi_2(\xi, 0) = \Psi_{2,\eta\eta}(\xi, 0) = \Psi_2(\xi, -\delta) = \Psi_{2,\eta}(\xi, -\delta) = \Psi_2(0, \eta) = \Psi_{2,\eta}(0, \eta) = 0, \tag{28}$$

$$\Psi_2(1, \eta) = 2 \sum_m \sum_n (D_{mn} \mathrm{Sh}(A_m + A_n)\eta + D^*_{mn} \mathrm{Sh}(A_m - A_n)\eta) J_0(A_m) J_0(A_n), \tag{29}$$

$$\Psi_{2,\xi}(1, \eta) = \sum_m \sum_n (H_{mn} \mathrm{Sh}(A_m + A_n)\eta + H^*_{mn} \mathrm{Sh}(A_m - A_n)\eta) J_0(A_m) J_0(A_n), \tag{30}$$

$$H_{mn} = 4D_{mn} - D_{mn} E_{mn} (A_m^2 - A_n^2),$$
$$H^*_{mn} = 4D^*_{mn} - D^*_{mn} E^*_{mn} (A_m^2 - A_n^2), \qquad J_{on} = J_o(A_n \xi), \qquad J_{1n} = J_1(A_n \xi).$$

The biorthogonal eigenvalue problem (23, 24, 25, 26) has the solution

$$\Psi_1(\xi, \eta) = \sum_{-\infty}^{\infty} \frac{\hat{C}_n \, \mathrm{e}^{P_{n\xi}\eta} + \hat{D}_n \, \mathrm{e}^{-P_{n\xi}\eta}}{P^2_{\eta\xi}} \phi_{n\xi}(\xi; P_{n\xi}), \tag{31}$$

with the eigenfunction

$$\phi_{n\xi}(\xi; P_{n\xi}) = -\xi J_0(P_{n\xi}) J_1(P_{n\xi}\xi) + \xi^2 J_1(P_{n\xi}) J_0(P_{n\xi}\xi). \tag{31a}$$

The complex eigenvalues $P_{n\xi}$ are the roots of

$$J_1^2(P_{n\xi}) + J_0^2(P_{n\xi}) - \frac{2}{P_{n\xi}} J_0(P_{n\xi}) J_1(P_{n\xi}) = 0,$$

which assumes the asymptotic form

$$2P_{n\xi} = (2n - 1)\pi + i \ln[2(2n - 1)\pi], \qquad \bar{P}_{n\xi} = P_{-n\xi}, \quad n = 1, 2, \ldots, \infty.$$

The eigenvalue problem (27, 28, 29, 30) is satisfied by

$$\Psi_2(\xi, \eta) = \sum_{-\infty}^{\infty} \frac{C^*_n}{P^2_{n\eta}} \xi I_1(P_{n\eta}\xi) \phi_{n\eta}(\eta; P_{n\eta}), \tag{32}$$

with the modified Bessel function of the first order $I_1$ and the eigenfunction

$$\phi_{n\eta}(\eta; P_{n\eta}) = X_n \cos X_n \sin P_{n\eta}\eta - \eta P_{n\eta} \sin X_n \cos P_{n\eta}\eta. \tag{32a}$$

The complex eigenvalues $P_{n\eta}$ are the roots of

$$\sin X_n = 2X_n, \qquad X_n = P_{n\eta}\delta, \qquad \bar{P}_{n\eta} = P_{-n\eta}, \quad n = 1, 2, \ldots, \infty.$$

Complex biorthogonal series solutions of the type (31, 32) have been used before in various types of fluid and solid mechanics problems by Joseph and co-workers, and a summary given by Joseph [14]. Convergence theorems for expansions of the types (31) and (32), in the case

of canonical data, are given by Joseph et al. [15]. When the data is not canonical, as is the case in this paper, convergence in the interior and to boundary data is established numerically in the literature. But, it is shown that whenever convergence to boundary data is obtained a set of compatibility conditions are satisfied. These conditions take the following forms for the problems of the type (23) and (27)

$$\mathcal{F}_1(\xi) = \xi\left(\frac{1}{\xi}\Psi_{1,\xi}(\xi, -\delta)\right)_{,\xi},$$

$$\langle \mathcal{F}_1(\xi)\rangle = \langle \xi^2 \mathcal{F}_1(\xi)\rangle, \qquad \langle \cdot \rangle = \int_0^1 \frac{1}{\xi}(\cdot)\,d\xi, \tag{33}$$

$$\mathcal{F}_2(\eta) = \Psi_{2,\eta\eta}(1, \eta),$$

$$\langle \mathcal{F}_2(\eta)\rangle = \langle \eta \mathcal{F}_2(\eta)\rangle = 0, \qquad \langle \cdot \rangle = \int_{-\delta}^{\delta} (\cdot)\,d\eta. \tag{34}$$

Condition (25) on the bottom cover for the radial direction eigenvalue problem for $\Psi_1$ does not satisfy (33). Thus the prescribed data on the bottom cap is not compatible with the side wall conditions in (24). Similarly, although (32) satisfies the governing equation (27) and the coefficients in the series are determined through biorthogonality, the prescribed data on the side walls given by (29) and (30) cannot be expanded in a series of the form (32) because (29) violates (34). However, our numerical experiments indicate that the data is actually quite well approximated over 90% of both the bottom cover and the side wall with the exception of the neighborhood of the corner $(1, -\delta)$. Consequently, the series (31) and (32) should approximate the solution rather well in the interior, away from the corner $(1, -\delta)$. That this is indeed the case is verified by checking the complex biorthogonal series solution with the numerical solution via the algorithm given in section II.2.1.

Available evidence indicates, in semi-infinite strip problems for instance, that the inclusion of the eigenvector corresponding to the zero eigenvalue into the series (31) and (32) may complete the eigenvector space and ensure convergence to data. That eigenvector is excluded from (31) and (32) because the eigenvalue zero is not compatible with either (33) or (34). Thus we conclude that the eigenvector sets (31a) and (32a) are quite possibly incomplete and do not span the solution spaces of problems (23–26) and (27–30), respectively. The above presentation serves a purpose because it may very well be a matter of constructing the eigenvector corresponding to the zero eigenvalue for the eigenvector set to form a basis, and force the series (31) and (32) to converge uniformly to the prescribed data.

In the absence of uniform convergence to data we solved instead (21a,b,c) by a numerical algorithm appropriate for the Stokes-Beltrami operator $L$ in (21a). The use of a numerical solution for the meridional field serves two purposes. Firstly, the influence of the singularity on the flow field, in particular, in the neighborhood of the singularity itself, should be represented in the best possible way. And secondly, how well and over how large a region the complex biorthogonal series solution approximates the real physical flow field should be checked based on a comparison with the numerical solution. Checking the numerical solution against the series solutions (31) and (32) shows that, indeed, the convergence of the series over most of the flow domain and, in particular, in the interior is quite rapid and close to the numerical solution except in the neighborhood of the singularity in a way similar to the Saint-Venant effect in elasticity. Next we present the details of the numerical algorithm.

*II. 2.1 Numerical algorithm*

Consider an equation of type $(21a)_1$

$$L^2\Psi = f \quad \in D\,, \tag{35}$$

where $L$ is a linear, second order operator with

$$\Psi_{,n}|_{\partial_1 D} = g\,, \qquad \Psi_{,nn}|_{\partial_2 D} = l\,, \qquad \partial_1 D \cup \partial_2 D = \partial D\,, \tag{36}$$

$n$ represents the normal direction to the boundary $\partial D$, and if $\Psi$ is taken as the stream function the conditions $(36)_1$ and $(36)_2$ are equivalent to specifying the velocity on $\partial_1 D$ and the shear traction on $\partial_2 D$. Although (35) and (36) can be solved by a straightforward application of finite difference methods, the direct inversion of the matrix to solve the resulting linear algebraic equations may be prohibitive for high accuracy in some cases without a supercomputer. Iterative methods for such fourth order equations converge rather slowly and in some cases not at all. We develop a method which is considerably more efficient than other iterative methods known to us. Convergence is faster and overall computational demands, i.e. computer time and memory, is much less.

It is well known that the numerical solution of incompressible flows poses a special challenge, in that the mass conservation equation and the pressure require special attention. Usually some form of the momentum balance evaluated at the boundary is used as a kinematic condition there in finite difference computations. But, this procedure does not necessarily guarantee the satisfaction of the incompressibility condition at the wall. The lack of a physical pressure boundary condition compounds the problem. Kleiser and Schumann [16] devised a method based on the Poisson equation for the pressure to satisfy the kinematical conditions at the wall. They use the matrix influence technique of Buzbee et al. [17] to generate pressure boundary conditions which imply satisfaction of the mass conservation at the wall. The numerical algorithm used in this paper has similarities with Kleiser & Schumann's but is completely different in essence.

We develop an efficient iteration method based on the Stokes-Beltrami operator, and use a matrix influence technique to generate conditions for one of the dependent variables. Specifically, two coupled, second order, nonhomogeneous partial differential equations of the Stokes-Beltrami type, equivalent to the fourth order problem (35), are solved iteratively, and the boundary conditions for one of the equations in the set are generated at each step of the iteration by a matrix influence technique.

Express (35) as

$$L\phi = f\,, \qquad L\Psi = \dot{\phi}\,. \tag{37}$$

$(37)_1$ can be solved subject to $(36)_2$

$$\Psi_{,nn}|_{\partial_2 D} = l = L\Psi|_{\partial_2 D} = \phi|_{\partial_2 D}\,, \tag{38}$$

which provides a direct condition for $\phi$ on $\partial_2 D$, and subject to $(36)_1$ which does not provide a direct condition for $\phi$ on $\partial_1 D$. It is necessary to choose $\phi$ on $\partial_1 D$ such that $(36)_1$ is satisfied. Let there be $N$ boundary nodes on $\partial_1 D$. At each node $\Gamma_i$, $\phi_i$ is sought such that

$$\Psi_{,n}|_{\Gamma_i} = g_i\,, \qquad \Gamma_i \in \partial_1 D\,.$$

For an arbitrary $\phi_i^0$, however,

$$\Psi_{,n}|_{\Gamma_i}^0 \neq g_i \, .$$

The superscript (0) denotes the old value of $\Psi_{,n}$ found while using the old $\phi_i^0$. A new set of values of $\phi_i$ is sought such that

$$\Psi_{,n}|_{\Gamma_i}^n = g_i \, ,$$

where the superscript ($n$) stands for new. This new value of $\Psi_{,n}$ can be expressed in terms of a Taylor series

$$\Psi_{,n}|_{\Gamma_i}^n = \Psi_{,n}|_{\Gamma_i}^0 + \sum_{j=1}^{N} (\Psi_{,n}|_{\Gamma_i})_{,\phi_j}(\phi_j^n - \phi_j^0) + \cdots \tag{39}$$

This equation reflects the effect of changing the value of $\phi_j$ on the normal slope of $\Psi$ at a given node $\Gamma_i$. Changing any of the $N$ values of $\phi_j$ will effect the derivative at $\Gamma_i$ if the operator is elliptic. For a linear operator all higher order derivatives are zero. If the derivative in the summation in (39) can be found, a system of $N$ equations, one for each node point, will result for the $N$ unknowns $\phi_j$, $j = 1, \ldots, N$. The $\phi_j$ values which satisfy this system of equations result in the normal derivative of $\Psi$ at $\Gamma_i$ being equal to $g_i$.

Equations (37) are solved with some arbitrary appropriate value assigned to $\Psi \in \partial D$ and to $\phi \in \partial_2 D$. On $\partial_1 D$ all $\phi_i$ are set equal to zero. The values of all $\Psi_{,n}|_i^0$ at $\phi_j = 0$ are calculated using an appropriate finite difference approximation and stored. The boundary

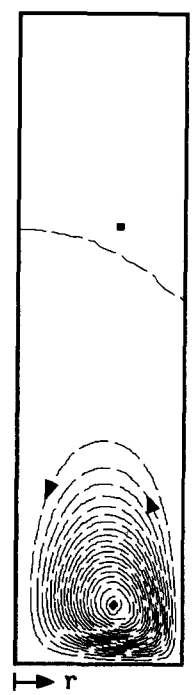


*Fig. 4.* Level lines of the dimensionless stream function $\Psi$ in the meridional plane for an aspect ratio of four. ■ = $0.0001543 \times 10^{-4}$, ◆ = $-4.129 \times 10^{-4}$.

value of $\phi_j$ is changed from zero to one and equations $(37)_1$ and $(37)_2$ are solved successively. The values of all $\Psi_{,n}|_i^1$ at $\phi_j = 1$ are calculated and stored. Since all higher derivatives are zero

$$\frac{\partial(\partial\Psi/\partial n|_i)}{\partial\phi_j} = \Psi_{,n}|_i^1 - \Psi_{,n}|_i^0 .$$

This yields all $N$ values of $\partial(\partial\Psi/\partial n|_i)/\partial\phi_j$. All $\phi_j$ values are reset to zero except for $\phi_{j+1}$ which is now changed to one. Equations $(37)_1$ and $(37)_2$ are again solved with these new boundary conditions. Following the above procedure, all $N$ of the values of $\partial(\partial\Psi/\partial n|_i)/\partial\phi_{j+1}$ at $\Gamma_i$ are found. All $N$ values of $\phi_j$ are sequentially modified to yield all $N$ times $N$ values of $\partial(\partial\Psi/\partial n|_i)/\partial\phi_j$. The solution of the system of equations

$$g_i - \frac{\partial\Psi}{\partial n}\bigg|_{\Gamma_i}^0 = \frac{\partial(\partial\Psi/\partial n|_i)}{\partial\phi_1}\phi_1^n + \frac{\partial(\partial\Psi/\partial n|_i)}{\partial\phi_2}\phi_2^n + \cdots + \frac{\partial(\partial\Psi/\partial n|_i)}{\partial\phi_N}\phi_N^n ,$$

$$i = 1, \ldots, N$$

yields the values of $\phi_i$ which give the appropriate normal derivative at the boundary. Since the derivative of $\Psi$ at a location $\Gamma_i$ is most strongly effected by the value of $\phi$ at the same location, the system of equations is diagonally dominant. As a result, either an iterative scheme or direct matrix inversion method can be used to find the solution.

Flow configurations numerically computed for representative cylinder aspect ratios are presented in Figs. 4–7 in $D_0$ together with some corresponding vorticity plots in Figs. 8 and 9.

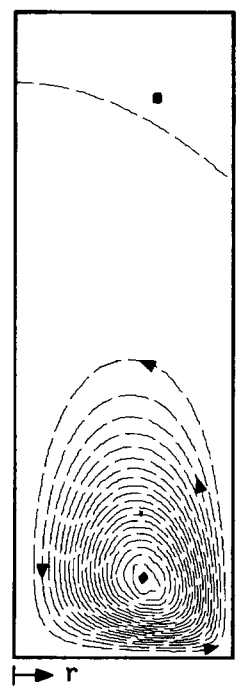


*Fig. 5.* Level lines of the dimensionless stream function $\Psi$ in the meridional plane for an aspect ratio of three. ■ = $0.000146 \times 10^{-4}$, ◆ = $-4.163 \times 10^{-4}$.

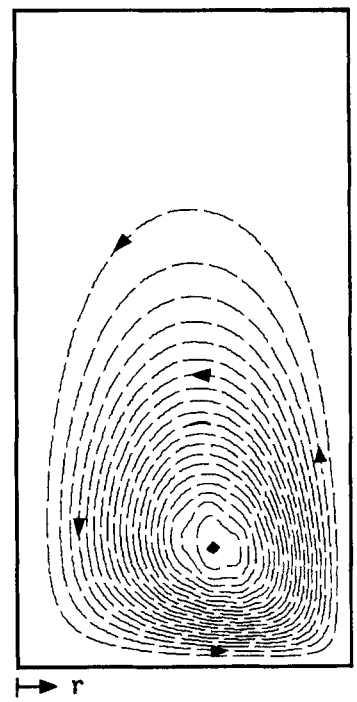


*Fig. 6.* Level lines of $\Psi$ for an aspect ratio of two. $\blacklozenge = -4.217 \times 10^{-4}$.

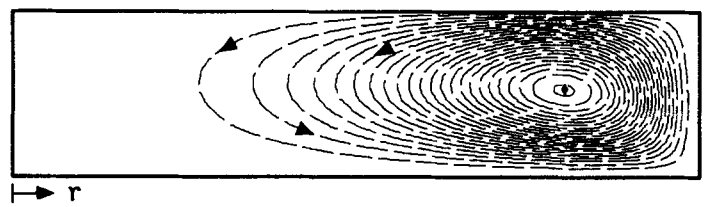


*Fig. 7.* Level lines of $\Psi$ for an aspect ratio of one fourth. $\blacklozenge = -4.632 \times 10^{-5}$.

The corresponding representations in the physical domain $D_\Omega$ can be obtained from Figs. 4–9 by inverting the one-to-one mapping $D_\Omega \rightarrow D_0$

$$\xi \rightarrow \frac{R}{a}, \qquad (\eta - H)\delta = \frac{Z}{a}(H + \delta), \tag{40}$$

given in terms of a dimensionless height rise coefficient $H$

$$2h = \Omega^2 h^{(2)} + O(\Omega^4), \qquad h^{(2)} = \frac{\rho a^4 H}{\sigma}. \tag{41}$$

The mapping (40) takes boundary points into boundary points. The level lines of $\psi$ in $D_\Omega$ are given by

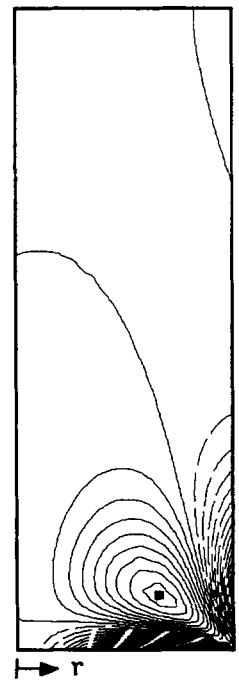


*Fig. 8.* Vorticity contours; aspect ratio three. ■ = $1.699 \times 10^{-2}$.

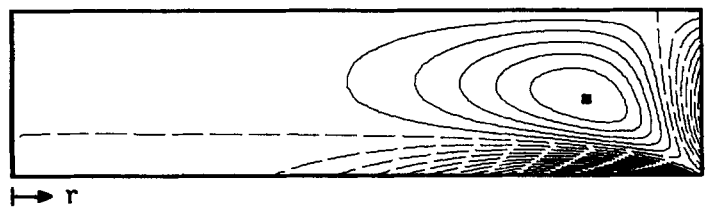


*Fig. 9.* Vorticity contours; aspect ratio one fourth. ■ = $1.199 \times 10^{-2}$.

$$2\psi(R, Z) = \Omega^2 \frac{\mathrm{d}^2}{\mathrm{d}\Omega^2} \psi(r, z)|_{\Omega=0} + O(\Omega^4)$$

$$\psi(R, Z) \simeq \frac{\rho a^5 \Omega^2}{2\mu} \Psi(\xi, \eta) = \frac{\rho a^5 \Omega^2}{2\mu} \Psi\left(\frac{R}{a}, \left[\frac{Z}{a}\left(\frac{H}{\delta} + 1\right) + H\right]\right).$$

### *II. 3. Interface shape*

The shape of the surface is determined by (11) which yields at this order

$$\frac{1}{\xi}(\xi H_{,\xi})_{,\xi} - \alpha^2 H = -\mathscr{P}(\xi, 0) + 2\frac{\Psi_{,\xi\eta}}{\xi}\bigg|_{\eta=0}. \tag{42}$$

Where the dimensionless height rise coefficient $H$ introduced in (41) and a dimensionless pressure field $\mathscr{P}$ have been used

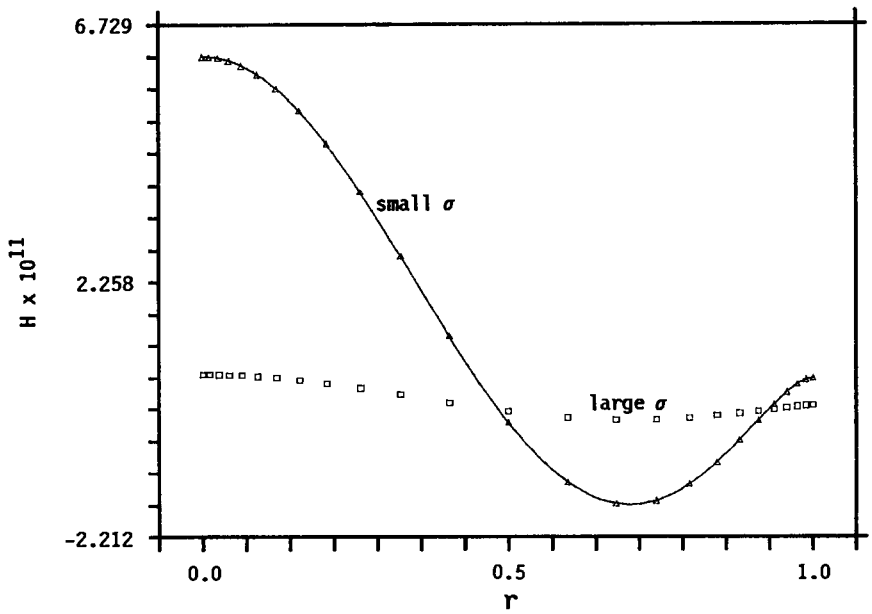


*Fig. 10.* Dimensionless free surface profile for an aspect ratio of four.

$$\mathscr{P} = \frac{\Phi^{(2)}}{\rho a^2}, \qquad \alpha^2 = \frac{\rho g}{\sigma} a^2 .$$

We neglect the static rise of the liquid at the wall of the cylinder and assume the angle of contact of the surface with the wall to be a right angle.

$$H_{,\xi}(1) = 0, \qquad H_{,\xi}(0) = 0 . \tag{43}$$

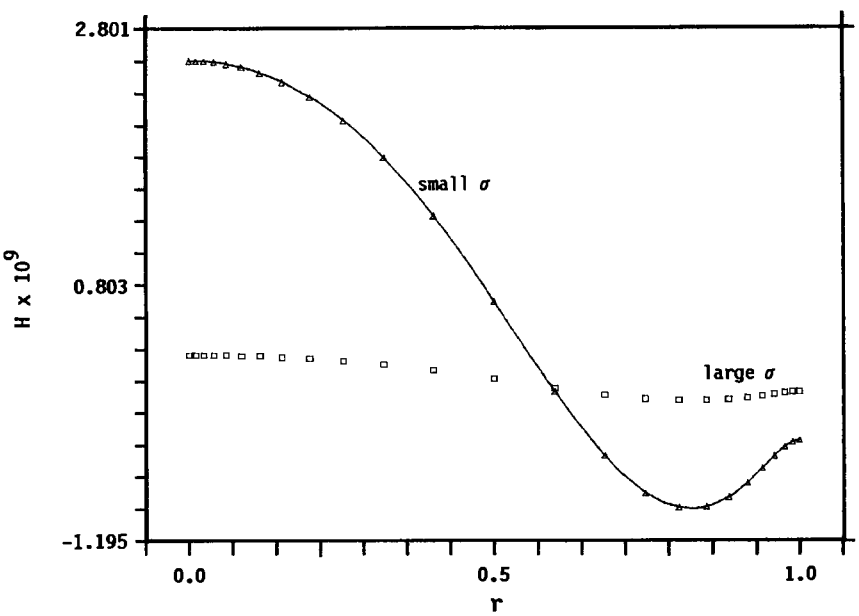


*Fig. 11.* Dimensionless free surface profile; aspect ratio three.

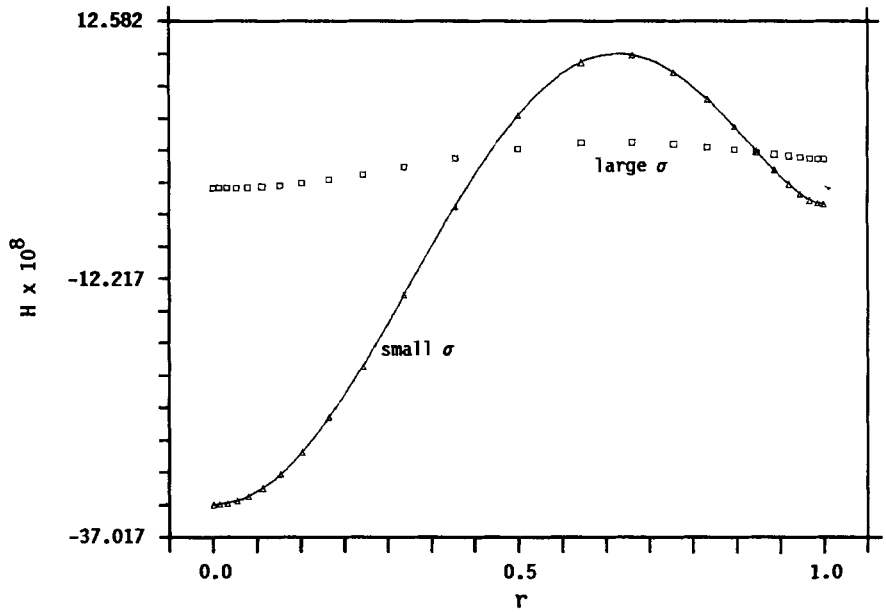


*Fig. 12.* Dimensionless free surface profile; aspect ratio two.

The second of (43) is required by symmetry. The pressure field $\mathcal{P}$ may be computed directly

$$\Delta\left(\frac{\Psi_{,\xi}}{\xi}\mathbf{e}_\eta - \frac{\Psi_{,\eta}}{\xi}\mathbf{e}_\xi\right) - \nabla\mathcal{P} = -2\frac{V^2}{\xi}\mathbf{e}_\xi\,,$$

$$\mathcal{P}(\xi,\eta) = -\frac{\Psi_{,\xi\eta}}{\xi} + \int^{\xi}\frac{\Psi_{,\eta\eta\eta}(s,\eta)}{s}\,\mathrm{d}s + 2\int^{\xi}\frac{V^2(s,\eta)}{s}\,\mathrm{d}s + C \tag{44}$$

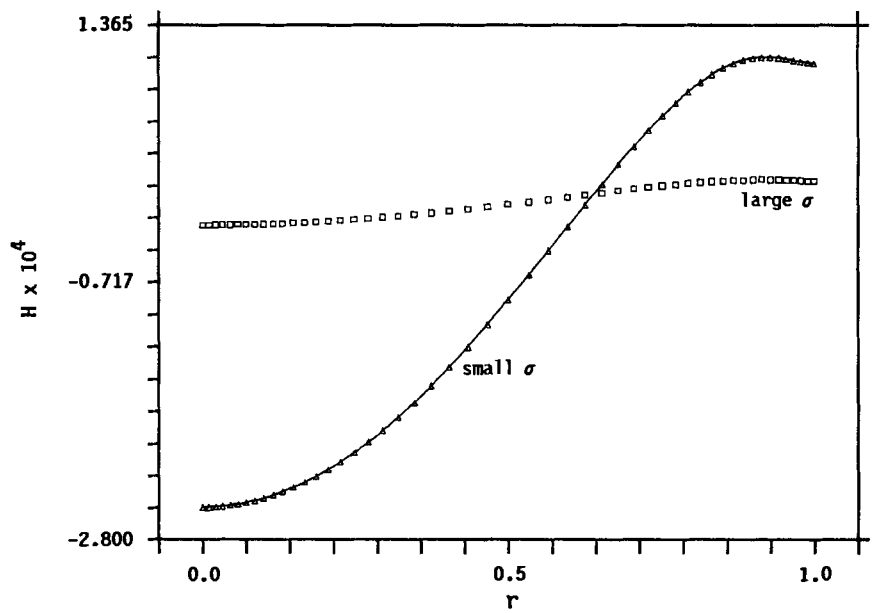


*Fig. 13.* Dimensionless free surface profile; aspect ratio one third.

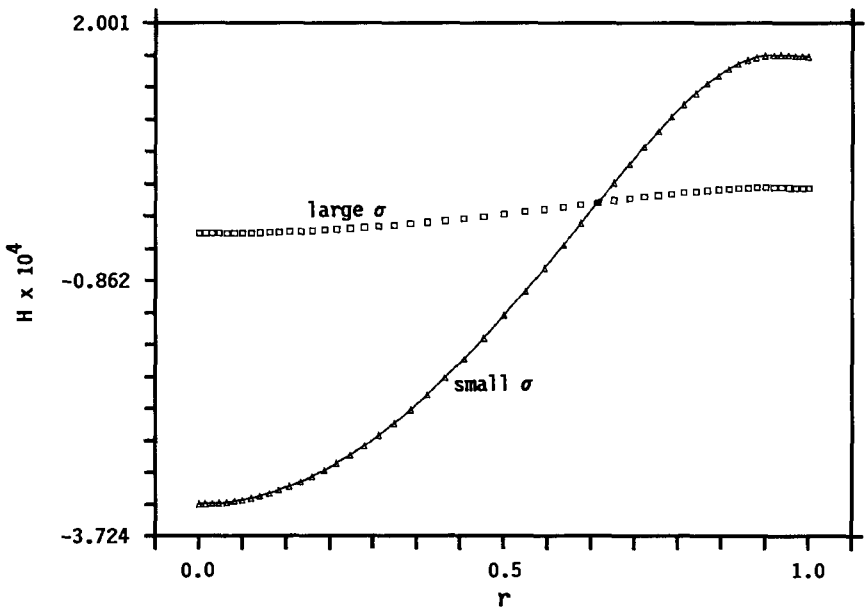


*Fig. 14.* Dimensionless free surface profile; aspect ratio one fourth.

The constant in (44) is determined through mass conservation (6) which yields at this order

$$\int_0^1 [\xi \mathscr{P}(\xi, 0) - 2\Psi_{,\xi\eta}(\xi, 0)]\, d\xi = 0 . \tag{45}$$

As $\Psi$ is available at the node points on the flat top of $D_0$, (44) and (42) are numerically integrated. Representative free surface shapes are given in Figs. 10–14 for those aspect ratios corresponding to the streamline plots of Figs. 4–7 and the aspect ratio one third for low and high values of the surface tension $\sigma$.

## III. Discussion

The flow field is shaped by the aspect ratio and the centrifugal forces. Liquid moves toward the corner on the bottom cap driven by the shear layer on the cover. The shear layer on the side wall moves the flow upwards toward the surface. Fluid particles cannot climb all the way to the interface if the cylinder is tall enough. Instead they turn radially inward on a toroidal trajectory. In the process they drag the particles closer to the top with them in the same direction and create a weaker clockwise rotating cell next to the interface, Figs. 4 and 5. The top eddy first appears for an aspect ratio slightly larger than 2 as a small top right corner eddy with stagnation points on the side wall and the free surface. At the same bottom cap angular velocity, as the aspect ratio increases towards three, $2 < \delta < 3$, the stagnation points migrate down the side wall and towards the axis of rotation, respectively. The stagnation point on the free surface migrates at a faster rate than the stagnation point on the side wall and quickly reaches the point $(0, 0)$ and starts moving down the axis of rotation towards the center $(0, -\delta)$ of the bottom cap. But, it stays always closer to the top than its counterpart

on the side wall. In Fig. 6 with $\delta = 2$ there is no corner or top eddy and in Fig. 5 with $\delta = 3$ the top stagnation point has already moved onto the centerline. For aspect ratios equal to and smaller than $\delta = 2$ there exists a single meridional cell. The radial velocities associated with this cell are very weak close to the top when the aspect ratio is close to two, either slightly larger or slightly smaller, Fig. 6. The single cell structure persists as the aspect ratio gets smaller and the region of quite weak circulation on top gradually disappears. For aspect ratios much smaller than one, $\delta \ll 1$, the cell develops strong circulation close to the side wall and very weak radial velocities close to the axis of rotation, Fig. 7. In fact the closer we get to the axis the weaker the velocities become.

For aspect ratios smaller than one half, level lines of the azimuthal velocity close to the axis of rotation are parallel to it indicating a horizontally stratified motion away from the side wall, much like Batchelor type rigid body motion between rotating disks, Fig. 3. For high aspect ratios, azimuthal velocity close to the top is almost nonexistent, Fig. 2, and there is a small inward radial velocity in the meridional plane, Fig. 6, suggesting a flow structure of the Stewartson type away from the bottom cover.

For tall cylinders, $\delta \geqslant 3$, there is a horizontally curved stagnation line on the side wall and a stagnation point on the centerline joined by a shear layer separating the top and bottom cells rotating clockwise and counterclockwise, respectively, in the meridional plane with upward and downward spiraling, toroidal particle trajectories in the top and bottom three dimensional cells. It is interesting that the taller the cylinder the closer is the non-horizontal shear layer separating the top and the bottom cells to the midplane.

The shape of the interface is determined primarily by the pressure field set up by the meridional cell structure. For tall cylinders the clockwise rotating top cell generates a pressure field of magnitude stronger close to the top and next to the axis of rotation. As a result the surface swells close to the symmetry axis and sinks next to the wall to satisfy mass conservation, Figs. 10 and 11. As the aspect ratio gets smaller the trough next to the wall moves closer to the wall, for instance in Fig. 10 for $\delta = 4$ the depression on the surface is further away from the wall than it is in Fig. 11 for $\delta = 3$. In both cases, note that the stagnation point is on the axis of symmetry, Figs. 4 and 5 respectively. In Fig. 5 ($\delta = 3$) it is closer to the top, increasing the magnitude of the peak swelling which occurs on the axis, Fig. 11, and pushing the depression closer to the side wall. For a large percentage of the interval between aspect ratios three and two the stagnation point is on top of the domain, moving towards the corner $(1, 0)$ as $\delta \to 2$. As a result the peak swelling on the surface migrates first towards the mid-span, and then past the mid-span towards the side wall always trailing the stagnation point. For $\delta = 2$, the two stagnation points, on the top of the domain and the side wall respectively, have already collapsed onto the corner $(1, 0)$, Fig. 6. The corresponding peak of the surface swelling is now located between the mid-span and the corner $(1, 0)$, with an almost vanished depression next to the wall, Fig. 12. As the aspect ratio gets smaller the peak moves closer to the wall under the effect of the pressure field set up by the single counterclockwise rotating cell. The smaller the aspect ratio the larger is the magnitude of the pressure field close to the wall, making the surface swell further as $\delta$ becomes smaller, Figs. 13 and 14, $\delta = 1/3$ and $1/4$ respectively. At the same time a negative gage pressure field is created between the mid-span and the axis of symmetry depressing the surface. This suction field reaches its maximum at the axis. The surface now behaves very much as intuition would have it, sinking at the axis and monotonically rising thereafter to reach the peak at the wall, Fig. 14. If surface tension is high the surface would be stiffer and

the magnitude of the corresponding deformation would be much reduced in all the cases, Figs. 10–14.

## Acknowledgement

We are indebted to the referee who pointed out to us the work of Kleiser and Schumann.

## References

1. T. Von Kármán, Uber laminare und turbulente Reibung. *ZAMM* 1 (1921) 233–252.
2. W.G. Cochran, The flow due to a rotating disc. *Proceedings of Cambridge Philosophical Society* 30 (1934) 365–375.
3. U.T. Bödewadt, Die Drehströmung über festem Grunde. *ZAMM* 20 (1940), 241–253.
4. G.K. Batchelor, Note on a class of solutions of the Navier-Stokes equations representing steady rotationally-symmetric flow. *Quarterly Journal of Mechanics and Applied Mathematics* 4 (1951), 29–41.
5. K. Stewartson, On the flow between two rotating coaxial discs. *Proceedings of Cambridge Philosophical Society* 49 (1953), 333–341.
6. J.F. Brady and L. Durlofsky, On rotating disk flow. *Journal of Fluid Mechanics* 175 (1987), 363–394.
7. P.J. Zandbergen and D. Dijkstra, Von Kármán swirling flows. In: J.L. Lumley, M. Van Dyke and H.L. Reed (eds), *Annual Review of Fluid Mechanics* 19 (1987), 465–491.
8. F. Schultz-Grunow, Der Reibungswiderstand rotierender Scheiben in Gehausen. *ZAMM* 14 (1935) 191–204.
9. H.P. Pao, A numerical computation of a confined rotating flow. *Journal of Applied Mechanics* 37 (1970), 480–487.
10. U. Cederlöf, Free-surface effects on spin-up. *Journal of Fluid Mechanics* 187 (1988), 395–407.
11. J. O'Donnell and P.F. Linden, Free-surface effects on the spin-up of fluid in a rotating cylinder. *Journal of Fluid Mechanics* 232 (1991), 439–453.
12. J.M. Hyun, Flow in an open tank with a free surface driven by the spinning bottom. *Journal of Fluids Engineering* 107 (1985), 495–499.
13. D.D. Joseph and L. Sturges, The free surface on a liquid filling a trench heated from its side. *Journal of Fluid Mechanics* 69 (1975), 565–589.
14. D.D. Joseph, A new separation of variables theory for problems of Stokes flow and Elasticity. In: *Trends in Applications of Pure Mathematics to Mechanics*. London: Pitman (1978) pp. 129–162.
15. D.D. Joseph, L.D. Sturges and W.H. Warner, Convergence of biorthogonal series of biharmonic eigenfunctions by the method of Titchmarsh. *Archive of Rational Mechanics and Analysis* 78 (1982), 223–274.
16. L. Kleiser and U. Schumann, Treatment of incompressibility and boundary conditions in 3-D numerical spectral simulations of plane channel flows. In: E.H. Hirschel (ed.), *Proceedings of the Third GAMM-Conference on Numerical Methods in Fluid Mechanics* (1980), V. 2, 165–172.
17. B.L. Buzbee, F.W. Dorr, J.A. George and G.H. Golub, The direct solution of the discrete Poisson equation on irregular regions. *SIAM Journal of Numerical Analysis* 8 (1971), 722–734.